Effect of ion bombardment on stress in thin metal films

S. G. Mayr[1,2,*] and R. S. Averback[2,†]
[1] *I. Physikalisches Institut, Georg-August Universität Göttingen, Tammannstrasse 1, 37077 Göttingen, Germany*
[2] *Department of Materials Science and Engineering, University of Illinois at Urbana-Champaign, 1304 W. Green Street, Urbana, Illinois 61801, USA*
(Received 8 August 2003; published 31 December 2003)

Ion-beam-irradiation-induced changes in the stresses operating in thin films are correlated with the thermodynamic phases of the films and the evolution in the film microstructures and morphologies. We investigate using a combination of experiments and molecular dynamics computer simulations the mechanisms that lead to residual stress changes in amorphous, nanocrystalline, columnar polycrystalline and single-crystal thin films. While local viscous relaxation within thermal spikes underlies all stress changes, i.e., a liquidlike region along the collision cascade, it can lead to very different states of stress in the different metallic films.

DOI: 10.1103/PhysRevB.68.214105 PACS number(s): 61.80.Jh, 61.82.Bg, 81.40.Lm

I. INTRODUCTION

MeV ion beam modification of surfaces and thin films has been the subject of extensive research activities during the past several decades.[1] While most early work with ion beams was concerned with the creation of point defects, defect reactions and impurity doping, newer work has addressed more the global response of solids under irradiation: phase stability in driven alloys,[2] evolution of surface morphologies,[3–6] and stress modification.[7–11] For the fields of thin films, surfaces, and nanotechnology, the ability to vary the stress in films presents new opportunities for tailoring the structure of thin films for specific applications, even after the sample has been prepared. In the present work we focus on the effect of ion beam bombardment on mechanical stresses in a variety of metallic thin film samples.

Irradiation of solids with energetic particles has been known for many years to alter the state of stress in bulk solids. This effect was attributed to the excess volumes of formation associated with irradiation-induced defects. Indeed, measurements of the change in lattice parameter[12] and change in stress[13] in single-crystalline solids have long been used to determine concentrations of point defects. It has also been known for nearly 20 years that irradiation with swift ions, i.e., ions having electronic stopping powers in excess of a few keV/Å, leads to plastic deformation of metallic glasses, with shrinkage in the direction of the beam and expansion transverse to it.[14] In thick specimens, or thin films on substrates, this effect can cause residual stress in the near-surface region. Lastly, we note that many amorphous samples, including covalent,[7] ionic,[8] and metallic[15] bonded solids, undergo stress relaxation during irradiation with ions at much lower energies, ranging from less than one keV to several MeV. Stress relaxation has been attributed to local melting and concurrent viscous flow in the vicinity of the ion track in densely packed materials,[16,17] a picture that emerges from molecular dynamics computer simulations.[18]

Due to their random nature as ''frozen liquids,'' the amorphous structure is usually considered a requirement for radiation-induced stress relaxation. This is based on the idea that local liquid regions along a thermal spike can rearrange and resolidify without strong boundary constraints being imposed by the surrounding crystalline material.[16] Specifically, lattice sites need not be conserved, and so atoms can rearrange to reduce stress. This is in obvious contrast to single-crystal samples where resolidification is nucleated by the surrounding crystalline lattice. In principle, defects created by the energetic recoil could organize to reduce the stress state, for example, in properly oriented dislocation loops, but there is currently no evidence for such behavior during low-temperature irradiation when defects are immobile. From the above discussion, it becomes clear that the primary requirement for stress relaxation in solid matter is the nonconservation of lattice sites. This condition is clearly met in amorphous materials, and not in single crystals. In the present work we examine this condition in detail, considering whether grain boundaries and surfaces can also influence changes in the stress state in irradiated materials, since the constraint imposed by the conservation of lattice sites is relaxed at these locations. The study described here employs a combination of experimental measurements and molecular dynamics (MD) computer simulations.

II. EXPERIMENTAL DETAILS

The measurements of the effects of irradiation on stress were performed on amorphous $Zr_{65}Al_{7.5}Cu_{27.5}$ and $Zr_{65}Cu_{35}$, nanocrystalline $Ag_{50}Co_{50}$, columnar polycrystalline Zr, and single-crystal Nb films. The amorphous films were vapor deposited on thermally oxidized Si(100) wafers using independently rate-controlled electron beam evaporators under UHV conditions (base pressure $p_B \leqslant 10^{-10}$ Torr). It is known from earlier studies that the stress evolution in glassy films during deposition is dependent on the alloy composition, and that it is overall tensile for $Zr_{65}Al_{7.5}Cu_{27.5}$ and compressive for $Zr_{65}Cu_{35}$.[19]

The Zr and $Ag_{50}Co_{50}$ films were grown under high vacuum (HV) conditions ($p_B \leqslant 10^{-8}$ Torr), also using rate-controlled electron beam evaporation and thermally oxidized Si(100) wafers. The α-Zr polycrystallites were (002) oriented, while the $Ag_{50}Co_{50}$ films were fcc with a (111) orientation. These crystalline films both develop tensile stresses during growth at ambient and liquid nitrogen temperatures, as determined from x-ray curvature measurements following

sample preparation.[20] This finding is in accordance with expectations for the growth of thick films by vapor deposition under conditions of low atomic mobility.[19,21,22] The intrinsic growth stress of $Ag_{50}Co_{50}$ at liquid-nitrogen temperature was so high that the film stress remained tensile even after warming to room temperature, despite the higher coefficient of thermal expansion of the metal film in relation to that of the Si substrate. Detailed x-ray studies with systematic variation of the substrate tilt out of the $\Theta-2\Theta$ geometry revealed a columnar microstructure for the Zr film and the nanocrystalline nature of the $Ag_{50}Co_{50}$ film. The Nb films were prepared with (110) orientation on sapphire (1120) substrates using molecular beam epitaxy (MBE). The substrate temperature during growth was ≈ 1160 K, although the sample was subjected to various annealing cycles after deposition. Details are found in Refs. 23 and 24.

The thicknesses of the substrates were kept thin, $\lesssim 200\ \mu$m, to ensure sufficient sensitivity to changes in the stress levels in the attached thin films. After preparation, the samples were mounted *ex situ* in a self-constructed three-capacitance dilatometer. Depth profiling by Auger electron spectroscopy (AES) and Rutherford backscattering (RBS) showed that the short exposure of the samples to air had no measurable effect on the results, as the samples were either sufficiently chemically inert (Nb, Ag, Co) or they passivate after the formation of a few monolayers of oxide (for samples containing Zr/Al).[25] The dilatometer simultaneously measures the distances between three reference plates and the back side of the samples at three locations using three separate capacitors and an ultrahigh-precision capacitance bridge (Adeen Hagerling, type 43532). This arrangement enables precise measurements of changes in the substrate curvature, since substrate tilts and shifts can be eliminated. The typical resolution of the dilatometer for the sample curvature measurements is $\geqslant 10$ km, where the limitations originate not from the capacitance measurement, but from mechanical vibrations in the experimental setup. Details on a similar system can be found elsewhere.[26]

The stress levels inside the films were calculated using the Stoney equation,[27] with the biaxial modulus for Si(100), $B_S = 1.805\times 10^{11}$ Pa,[28] the wafer thickness d_S, the film thickness d_F, and radius of curvature r,

$$\sigma = \frac{B_S d_S^2}{6 r d_F}. \tag{1}$$

While the described experimental apparatus provides an accurate measure of changes in the film stress, it does not yield the absolute level of stress in the film. We therefore measured the absolute stresses either by *in situ* stress measurements during film preparation (for the metallic glasses[19]) or by x-ray curvature measurements before (and after) ion irradiation. This latter approach provides a check on the relative stress levels obtained from the *in situ* capacitance measurements during irradiation. For determination of the stresses in the Nb film, we proceeded somewhat differently owing to the elastic anisotropy of the sapphire substrate. We thus determined the absolute stress levels directly from x-ray measurements of the lattice parameter perpendicular to the substrate, before and after ion beam irradiation. Comparison with the averaged values of the elastic constants in the (110) plane provided the absolute stresses in the films.

The ion beam irradiations were performed under HV conditions. Test measurements with different energies showed that if the ions crossed the film/substrate interface, a large increase in stress developed, which we attribute to ion beam mixing. Therefore the ion type and energy were optimized using SRIM simulations[29] to maximize the fraction of the sample being irradiated while preventing recoils from reaching the film-substrate interface.[30] 700 keV Kr^+ ions were employed for irradiation of the $Zr_{65}Al_{7.5}Cu_{27.5}$ and Zr films, 800 keV Kr^+ ions for $Zr_{65}Cu_{35}$ and $Ag_{50}Co_{50}$, and 700 keV Xe^+ ions for the Nb single-crystal films. The doses in all cases are converted to normalized units of displacements per atom (dpa) to enable comparisons between experiments and simulations, which have different irradiation parameters. A displacement energy[31] of 10 eV was employed in SRIM for the conversions from ion/cm^2 to dpa. The irradiations were performed at near-normal incidence, except for the case of Nb, for which the sample was tilted by $\approx 20°$ to avoid effects of channeling.

In addition to stress measurements, we determined using atomic force microscopy (AFM) the surface topography $h(\vec{x},t)$ [$\vec{x}=(x,y)$, where the x-y plane is parallel to the substrate] for representative doses and films. Our analysis is limited here to gray scale surface topographs and the rms (root mean square) roughness

$$\xi(t) = \sqrt{\langle [h(\vec{x},t) - \langle h(\vec{x},t)\rangle_{\vec{x}}]^2\rangle_{\vec{x}}}. \tag{2}$$

III. SIMULATIONAL DETAILS

The MD simulations were performed using PARCAS[32] with periodic boundary conditions imposed for the x and y directions, a free surface for the $+z$ direction, and three rows of fixed atoms at the bottom of the cell in the $-z$ direction, in analogy to a thin film on a substrate. The dimensions of the cell in the plane of the film were fixed and chosen to obtain the desired biaxial stress. To distinguish surface and substrate effects from bulk processes, we performed a second set of simulations employing periodic boundaries in all three directions, but with zero stress in the z direction. The cell contained a minimum of 25 atoms per electron volt of recoil energy and damping at the periodic boundaries to ensure realistic simulations of atomic recoils in a solid, i.e., to prevent significant heating of the simulation cell and to reduce possible effects of energy reflections at the boundaries. The temperature of the cell was initialized to 10 K and scaled during the recoil event toward this temperature at the three outermost layers abutting the periodic boundaries using a Berendsen thermostat.[33]

The atomic interactions were calculated using embedded atom method[34] (EAM) interatomic potentials with the short-range interaction fitted to the Ziegler-Biersack-Littmark universal repulsive potential.[35] The simulations considered the effect of recoils on biaxial stresses in amorphous $Cu_{50}Ti_{50}$, nanocrystalline $Ag_{50}Ni_{50}$, and single-crystal Cu. For $Cu_{50}Ti_{50}$ and Cu we used the potential formulated by Sabo-

chick and Lam[36] and for $Ag_{50}Ni_{50}$ the original Foiles EAM potential.[37] Both potentials have been shown to describe the relevant physical properties of these metals reasonably well, importantly here: the absolute magnitudes of the melting temperatures. The AgNi potential, however, underestimates the heat of mixing in the liquid, but this does not pose serious problems for the current purposes.[38]

The amorphous $Cu_{50}Ti_{50}$ simulation cell was created by successive annealing and quenching cycles until the potential energy no longer decreased. Evaluating the radial distribution function (absence of the second-nearest-neighbor peak) and locating the glass transition temperature during quenching verified the amorphous nature. The nanocrystalline $Ag_{50}Ni_{50}$ structure was created by simply placing 2 nm Ag and Ni nanocrystallites on a CsCl grid.[38] Since the structure is an ordered array of crystallites, each phase is interconnected through next-nearest-neighbor necks, which are a few tenths of nm in diameter. Before initiating the first recoil, the cell was relaxed to 10 K, during which time the Ag grains became far more distorted than the Ni grains. Presumably, the smaller elastic stiffness and stacking fault energy of Ag facilitate the formation of subgrains and twins, thus assimilating the stress level of the Ag and Ni grains. The Cu single crystal was created with a (001) surface. The in-plane lattice constant was set to its proper value for the applied stress.

The irradiation was performed by assigning a recoil energy to a randomly selected atom that was far from a damped or surface boundary. The direction of the recoil atom was also randomly chosen. Changes in the biaxial stresses were monitored as a function of the number of recoil events. In this context we note that during simulated irradiation no changes in the elastic properties were detected to within an uncertainty of $\approx 10\%$.

IV. RELAXATION OF GLASSY METAL FILMS

A. Experimental results

It is known from previous studies[19] that amorphous alloys that are grown by vapor deposition under UHV conditions develop a characteristic stress profile. Initially, the film obtains a stress that depends on the specific substrate, but as it grows thicker the stress becomes more compressive. At still greater thickness, the local state of stress changes to tensile again and then remains constant. The surface morphology in this latter stage of film growth is particularly rough. It is, in fact, the development of roughness that causes the tensile stresses. The characteristic thicknesses, the specific levels of stress, and the length scales of the roughness all depend on the specific alloy system.[39] For $Zr_{65}Al_{7.5}Cu_{27.5}$ the early- and late-stage stresses are tensile (-0.4 GPa and -0.58 GPa, respectively). The intermediate-stage stress is compressive (0.17 GPa) and extends from ≈ 20 nm film thickness to ≈ 220 nm. The average stress within the penetration depth of our 700 keV Kr^+ ions is tensile. The initial surface morphology in the late stages of film growth, moreover, is very rough, with huge domes ≈ 20 nm in diameter appearing in the AFM images.

For $Zr_{65}Cu_{35}$, the regime with compressive stresses prevails to the final film thickness, so that the overall irradiated region (800 keV Kr^+) is initially under compressive stress. It is noteworthy that due to the growth behavior of amorphous films, stress gradients in the irradiated region are unavoidable. For the present study, however, the combination of the film thickness and ion range resulted in the irradiated portion of the film being initially mostly homogeneously stressed.

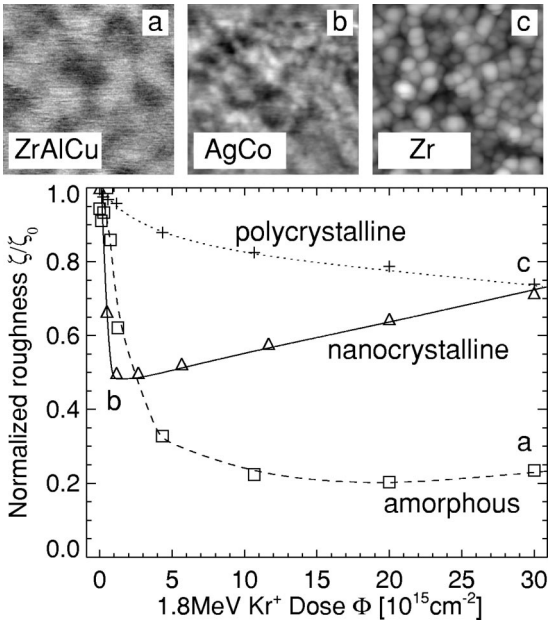

FIG. 1. Evolution of the surface morphologies of amorphous $Zr_{65}Al_{7.5}Cu_{27.5}$, nanocrystalline $Ag_{50}Co_{50}$, and columnar polycrystalline Zr films during 1.8 MeV Kr^+ ion beam irradiation. Ion bombardment of amorphous films enables the creation of atomically smooth films. Nanocrystalline films initially smoothen, but roughen for higher doses due to growth of surface grains. Columnar polycrystalline films hardly change the surface morphology during irradiation.

Figure 1 shows the dramatic smoothening reaction that occurs during bombardment of $Zr_{65}Al_{7.5}Cu_{27.5}$ films at ambient temperature.[3] The surface roughness, determined from AFM images, decreases rapidly at first, and then gradually reaches a minimum at $\approx 2\times 10^{16}$ ions/cm^2, when the films become almost atomically smooth. The intrinsic growth stress, on the other hand, relaxes almost completely by a dose of $\approx 5\times 10^{13}$ cm^{-2}, followed by a buildup of tensile stresses, which saturate by a dose of $\approx 8\times 10^{15}$ cm^{-2} at a level of ≈ -0.35 GPa (see Fig. 2).[40] Shown inset in Fig. 2 on an expanded scale are normalized stress relaxation curves at low doses for irradiations at three temperatures, ≈ 87 K, ≈ 300 K, and ≈ 607 K. The highest temperature is close to the calometric glass transition temperature T_G, which was determined to be ≈ 650 K for a heating rate of 20 K/min.[41] The radiation-induced viscosity (RIV), $\eta\dot{\Phi}$, was obtained from these data by assuming exponential relaxation behavior,[9,42] i.e.,

$$\frac{\sigma}{\sigma_0} = \exp\left(-\frac{B\Phi}{6\,\eta\dot{\Phi}}\right). \tag{3}$$

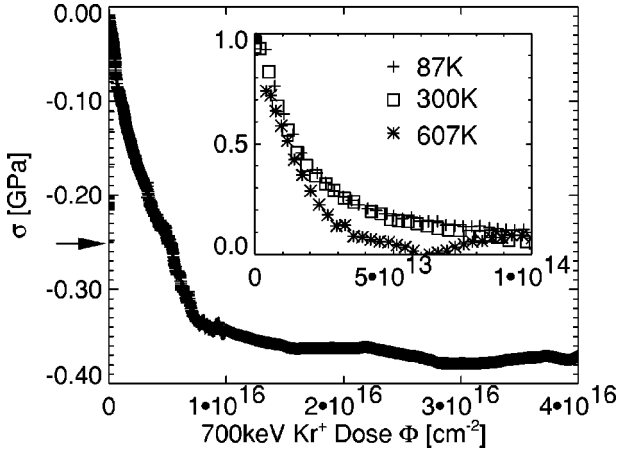

FIG. 2. Biaxial film stresses in $Zr_{65}Al_{7.5}Cu_{27.5}$ during bombardment with 700 keV Kr^+ ions. The arrow indicates the initial stress level. For low doses the stresses relax with an exponential decay (*inset*), which is measured temperature dependent and normalized to the initial stress. Only a weak temperature dependence is detectable.

Values of $(3.2\pm0.5)\times10^8$ Pa dpa, $(3.9\pm0.5)\times10^8$ Pa dpa and $(1.9\pm0.5)\times10^8$ Pa dpa for liquid-nitrogen temperature, room temperature, and 607 K, respectively, are determined, illustrating a very weak temperature dependence. A value of $\eta\dot{\Phi}=(8.5\pm4.25)\times10^8$ Pa dpa was obtained from measurements of surface smoothening using AFM,[3] which is in good agreement with the present stress relaxation measurements, considering the approximate nature of deducing viscosities from surface smoothening experiments.

Since stress relaxation is independent of the sign of the stress for Newtonian flow, it is useful to corroborate our interpretation of RIV by measuring stress relaxation on a sample that is initially under compressive stress as is the case for $Zr_{65}Cu_{35}$. These data are illustrated in Fig. 3 for a sample irradiated at room temperature. Again the radiation-induced viscosity was determined by fitting Eq. (3) at low doses, with the result that $\eta\dot{\Phi}=(2.7\pm0.5)\times10^8$ Pa dpa. Within the uncertainties, this value is in agreement with the measurement on $Zr_{65}Al_{7.5}Cu_{27.5}$, and thus an indication that radiation-induced flow is indeed Newtonian. Continued irradiation of $Zr_{65}Cu_{35}$ films to high doses results in tensile stresses with a saturation value of ≈-0.42 GPa, which is also quite similar to the value observed in $Zr_{65}Al_{7.5}Cu_{27.5}$. It is noteworthy, however, that the dose required to reach the saturation stress is considerably higher for $Zr_{65}Al_{7.5}Cu_{27.5}$ than for $Zr_{65}Cu_{35}$, even though their radiation-induced viscosities are nearly the same.

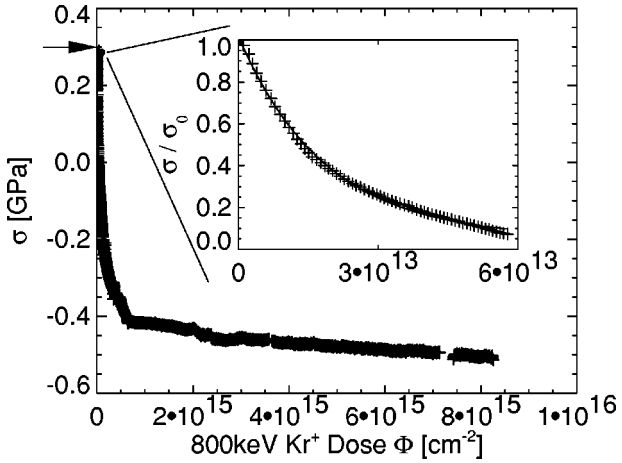

FIG. 3. Biaxial film stresses in $Zr_{65}Cu_{35}$ during irradiation with 800 keV Kr^+ ions. For low doses the stress relaxation follows an exponential decay (*inset*).

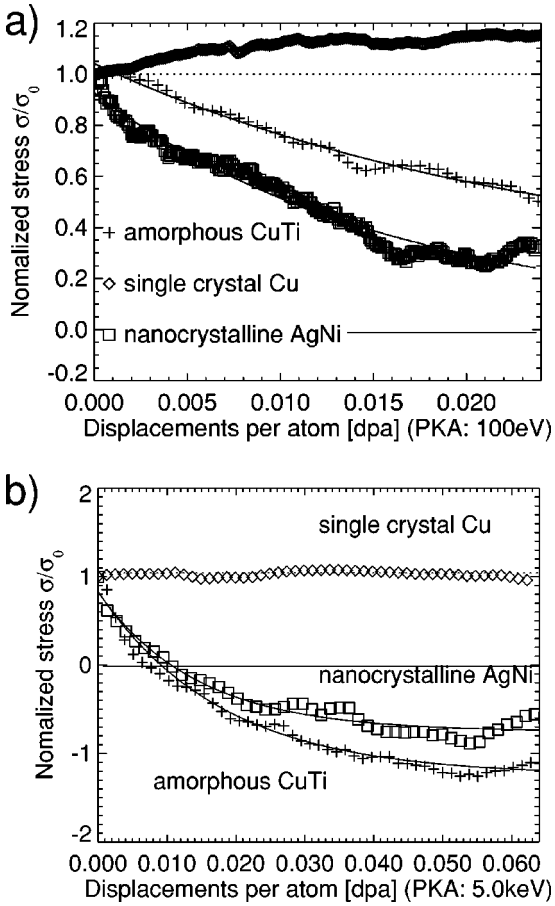

FIG. 4. MD simulation of the relaxations of the normalized biaxial film stresses σ/σ_0 by (a) 100 eV and (b) 5 keV primary knock-on atoms (PKA): Stress relaxation is only observable for amorphous and nanocrystalline films, and does not occur for single-crystal Cu films. Instead compressive stress is built up for 100 eV recoils in Cu due to defect generation. The exponential fits are employed for the determination of the (effective) radiation-induced viscosity.

B. Simulations and discussion

MD simulations of radiation-induced viscous flow were performed on three metal systems: amorphous $Cu_{50}Ti_{50}$, nanocrystalline $Ag_{50}Ni_{50}$, and single-crystalline Cu. Representative results for all three structures are shown in Fig. 4 for two different recoil energies, 100 eV and 5 keV. For the present we confine our discussion to amorphous $Cu_{50}Ti_{50}$. For this glass, local melting within a thermal spike is ob-

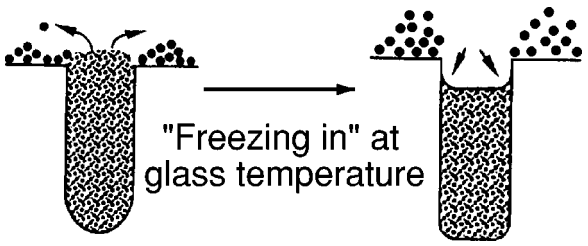

FIG. 5. Illustration of the mechanism of tensile stress generation in amorphous and nanocrystalline samples during ion irradiation.

served only for 5 keV recoils; the 100 eV recoils only create point defects (see also Ref. 9). For both energies, however, the initial state of stress undergoes relaxation. Two sets of boundary conditions were examined; the first—as shown in Fig. 4—employed periodic boundaries in x-y, a free surface in $+z$, and a substrate in the $-z$ direction, in analogy to the experimental film geometry. The other employed periodic boundaries in all three directions, i.e., a bulk specimen, but we maintained zero stress in the z direction. For the 100 eV recoils, the relaxation rate of the initial stress was the same for the two boundary conditions. For the 5 keV recoils, on the other hand, the rates and final stress levels differed, indicating the onset of additional surface-related mechanisms. We therefore first consider stress relaxation in the bulk geometry. Applying Eq. (3) on the relaxation curves yields the RIV's, which are similar for the two energies, when compared on the basis of defect production: 3.9×10^{8} Pa dpa and 3.6×10^{8} Pa dpa for 100 eV and 5 keV recoils, respectively. The good agreement of these calculated numbers with the experimental data corroborates our viewpoint expressed previously[9] that defects create local shear instabilities in an amorphous matrix, and this mediates viscous flow.

The simulations of 5 keV recoils using the boundary conditions of a thin film, Fig. 4(b), show that, similar to the experiments, significant tensile stresses develop during bombardment and that they appear to saturate at high doses. The absolute saturation level of stress, ≈ -0.49 GPa, is even in good quantitative agreement with the experiments. Visual inspection of the simulation cell reveals the origin of this tensile stress (Fig. 5), viz., the elevated temperature within thermal spikes creates high pressures, due to thermal expansion, and this leads to material flow onto the surface. Upon cooling, the material contracts, but when it cools below the glass transition temperature the flow is suppressed. Hence, on further cooling to ambient temperature, tensile stresses are generated owing to the thermal contraction. For high recoil energies the number of atoms remaining above the surface, as a bump, is much larger than the sputtering yield. Recoils as low in energy as 5 keV in $Cu_{50}Ti_{50}$, for example, are found in our simulations to produce more than an order of magnitude more adatoms than sputtered atoms.

A simple model calculation illustrates the plausibility of our proposed mechanism. Once the entire film has been overlapped with thermal spikes several times, we expect the stress in the film to reach a steady state value given by

$$\sigma \approx B\nu\Delta T \approx -0.42 \ \text{GPa}, \tag{4}$$

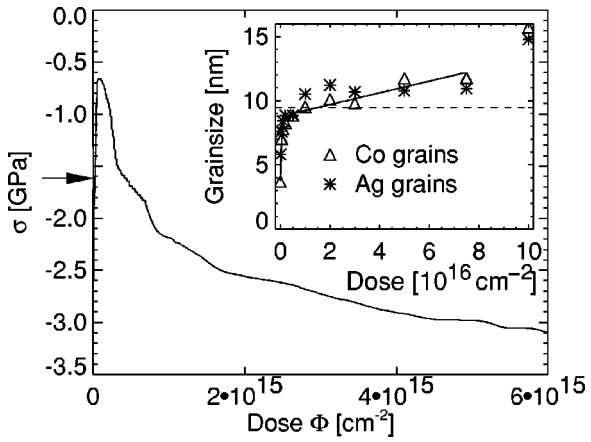

FIG. 6. Stresses in nanocrystalline $Ag_{50}Co_{50}$ films relax at small doses ($\lesssim 2\times10^{14}$ cm^{-2}) and get strongly tensile at higher doses. For $\Phi \gtrsim 2\times10^{15}$ cm^{-2} the tensile stress increases almost linearly as a function of dose. This behavior is accompanied by grain growth, as shown in the *inset*. Once the size of the thermal spike (dashed line) is exceeded, the thin film kinetics decelerates markedly. The doses are measured with or are normalized to 1.8 MeV Kr^{+} ions.

where we employed[43] the biaxial modulus $B\approx140$ GPa, the thermal expansion $\nu\approx1\times10^{-5}$ K^{-1} and the temperature difference between glass transition and substrate temperature $\Delta T\approx-300$ K. This value of stress is in good agreement with both simulations and experiments. Concerning stress relaxation, it is clear that the above mechanism for generating tensile stress is additive with stress relaxation to reduce the incipient compressive stresses. The effective radiation-induced flow [Fig. 4(b)], therefore, becomes non-Newtonian and the RIV is reduced (2.8×10^{8} Pa dpa). A free-standing film shows even greater reduction of the RIV,[9] illustrating the effect of the constraints imposed on the film by the substrate.

V. STRESS RELAXATION IN NANOCRYSTALLINE FILMS

A. Experimental results

Our experimental results on stress relaxation on initially nanocrystalline $Ag_{50}Co_{50}$ films have been reported previously;[38] however, we briefly summarize them here to provide a broader context of stress relaxation in metals. As illustrated in Figs. 1 and 6, grain growth, surface smoothing, and stress relaxation in nanocrystalline $Ag_{50}Co_{50}$ are strongly correlated. Rough surfaces smoothen, tensile stresses relax, and grains grow, and all very rapidly when the grain size is smaller than the size of the thermal spike (≈9 nm for doses $\Phi\lesssim1\times10^{14}$ cm^{-2}). We attributed this behavior to the presence of many grain boundaries within the thermal spike, which allow for the nonconservation of lattice sites. For grain growth, for example, we noted that owing to the immiscibility of Ag with Co in both the solid and liquid phases, grain boundary migration and bulk diffusion mechanisms were suppressed, and that a sinteringlike mechanism was necessary.[38,44] For liquid phase sintering, however, it is necessary that significant regions around triple junctions are melted, and this becomes increasingly less likely as the grain

size grows larger than the size of the thermal spike. As a consequence, more and more overlaps of cascades are required, as indicated in Fig. 6, thus markedly increasing the effective radiation-induced viscosity.

From an analysis of the grain growth, surface, and stress relaxation data we found in the regime of small grain sizes values of RIV of 2.15×10^8 Pa dpa, 2.8×10^8 Pa dpa, and 8.8×10^9 Pa dpa, respectively. The values calculated from surface relaxation and grain growth agree well with each other and with the value obtained for the amorphous metals. The stress relaxation measurements showed a higher value, i.e., it proceeds more slowly. We tentatively attributed this difference to the fact that changes in stress can derive from sources in the complex microstructure other than simple stresses relaxation. For example, the concomitant growth of grains can create tensile stresses, and possibly the surrounding crystalline matrix imposes constraints that are typical of single-crystalline materials (see below). The details of these processes, however, are not presently understood.

Measurements of the rate of grain growth at high doses yielded a value of RIV of $\approx9.6\times10^9$ Pa dpa. We noticed too a strong buildup of tensile stresses at high doses, similar to the observation for the glassy films, and we interpret it, at least partially, on the same basis, material flow onto the surface. Additional mechanisms additionally have to be expected to contribute, for example, densification of the film during grain growth is suggested by the rapid increase in tensile stress with increasing grain size, (see Fig. 4). At higher dose, the rate of grain growth slows as does the rise in tensile stress. Ion beam mixing in combination with deviations from Vegard's law is also capable of generating stresses, although these particular stresses are expected to be an order of magnitude smaller.[45]

B. Simulations and discussion

In our previous study, we performed MD simulations at high energy, 20 keV,[38] where several grains undergo melting simultaneously. The present work complements that investigation by simulating stress relaxation in nanocrystalline $Ag_{50}Ni_{50}$ subjected to 100 eV and 5 keV recoil events. Thermal spikes are typically the size of a nanograin ($\approx$3000 atoms) for 5 keV recoils, while for 100 eV events, melting was not observed. The new results are shown in Fig. 4. For 5 keV recoil energy, the results for the AgNi simulation cell with the open-surface geometry [Fig. 4(b)] show a clear similarity with amorphous $Cu_{50}Ti_{50}$, which we interpret accordingly, i.e., stress relaxation by radiation-induced viscous flow at low doses followed by the creation of tensile saturation stresses (-0.21 GPa) at higher doses, due to the flow of material onto the surface. We can now rule out the possibility that these tensile stresses arise from grain growth, since additional simulations using the bulk sample geometry, with zero applied pressure in the z direction, resulted in a saturation tensile stress that was one order of magnitude smaller (≈-0.04 GPa). The RIV for thin-film geometry, 2.33×10^8 Pa dpa, is about a factor of 2 higher than that for the bulk geometry (1.23×10^8 Pa dpa). We tentatively attribute this small difference to constraints imposed on the thin-film geometry by the substrate. Recall that in the thin-film geometry, atoms in the surface in the $-z$ direction are held fixed. This result contrasts with that from the amorphous samples, where the relief of constraints by the open surface dominates over the presence of the substrate, and it suggests that the inherent crystal lattice of the grains restricts the reordering process when only a few grains are melted. We also note that the experimental RIV is significantly larger than that found by the simulations. This appears to be an artifact of the ordered CsCl grain structure employed in our simulation cell, which allows for efficient stress relaxation. In fact, even for 100 eV recoils, stress relaxation in the nanocrystalline simulation cell remains efficient (RIV, 2.60×10^8 Pa dpa); this efficiency appears to arise from the relief of stress by the rotation of grains. This is shown by the displacement fields in Fig. 7. This mechanism of grain rota-

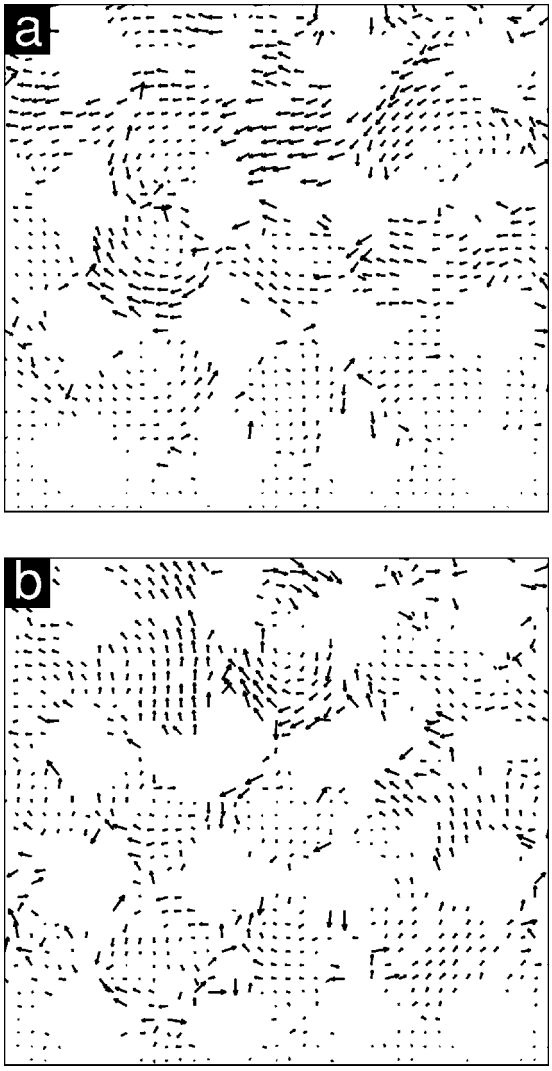

FIG. 7. Grain rotation during 100 eV irradiation of AgNi films that are initially under (a) compressive (0.5 GPa) and (b) tensile (-0.5 GPa) biaxial stresses: The displacement fields of the atoms in the plane of the biaxial stress are calculated after 180 recoils ($\approx$0.017 dpa). Stresses are relaxed by rotation of the (nonspherical) grains in an appropriate direction. Here only the $+z$ surface is open; the atoms at the $-z$ surface are fixated.

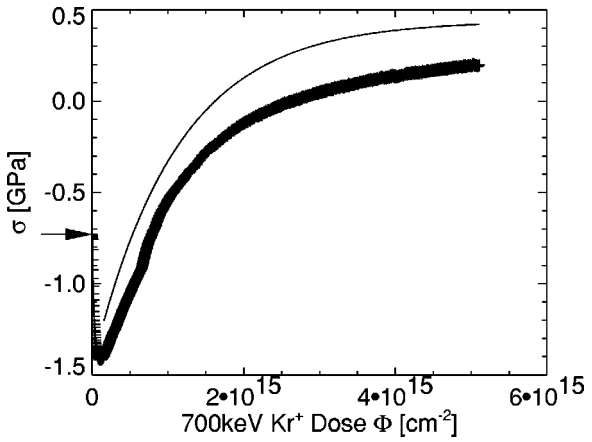

FIG. 8. Biaxial film stresses during bombardment of a columnar polycrystalline Zr film with 700 keV Kr^+ ions: The initial tensile stress increases at low doses and reaches a maximum at ≈ -1.45 GPa. For higher doses, the stress trends exponentially towards a compressive saturation value at ($\sigma \approx 0.245$ GPa)—see fitting curve.

tion is reversible with stress inversion, but it strongly depends on the presence of open surfaces. The elimination of open surfaces (by choosing a fully periodic simulation cell) leads to a remarkable deceleration of stress relaxation, as is quantitatively visible from a strongly elevated RIV (1.15×10^9 Pa dpa). Nevertheless, stress relaxation by grain rotation can be expected to be relevant experimentally for certain grain geometries.

VI. STRESS RELAXATION IN COLUMNAR POLYCRYSTALLINE FILMS

A. Experimental results

At ambient temperature, α-Zr films grow in a polycrystalline columnar microstructure. AFM surface topographs of the *as prepared* films show the top domes of these columns, which have a diameter of ≈ 30 nm [similar to Fig. 1(c)]. The stress profile in a film grown with a columnar structure is well established,[20–22] following the same scheme as described above for amorphous film growth [for a schematic drawing see Fig. 9(d)]. The type of stresses that develop in the early stages of growth depend on the specific substrate. The next stage of growth is characterized by compressive stress, although it eventually changes to tensile stress with continued growth. The region that is accessible to 700 keV Kr^+ irradiation is expected to contain a stress gradient, with the highest tensile stresses close to the surface, and a reduced tensile or even compressive stress near to the penetration depth of the ions.

As Fig. 1 shows in the AFM images, ion irradiation has only a minor influence on both the surface roughness and diameters of the top domes of the columns, i.e., it does not much modify the column grain sizes. The dependence of the biaxial film stresses on irradiation dose is shown in Fig. 8. For low doses $\lesssim 2 \times 10^{14}$, a strong increase in the magnitude of the tensile stresses is observed (up to ≈ -1.45 GPa). This is followed by an exponential decrease in stress, which finally results in the generation of compressive stresses and a final value of ≈ 0.245 GPa. The transition from tensile to compressive stress occurs at a dose of $\approx 3 \times 10^{15}$ cm^{-2}.

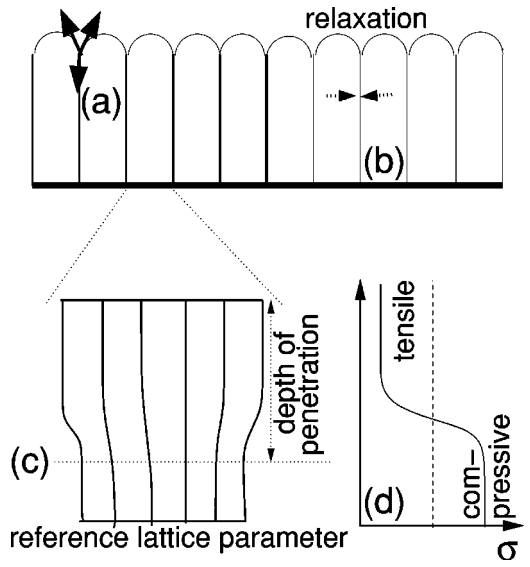

FIG. 9. In columnar polycrystalline films two mechanisms appear to contribute to stress generation during irradiation. First, grain boundary relaxation leads to a densification of the film and therefore to tensile stresses. Second, successive melting and crystallization within thermal spikes drives the lattice parameter of the columns toward its value at the penetration depth of the ions (c,d). Depending on the initial state of the film, therefore, the resulting stresses can be tensile or compressive.

B. Discussion

The experimental results on stress modification of columnar polycrystalline Zr by ion bombardment are, at first glance, in strong contrast to those for the nanocrystalline and amorphous films. Neither surface smoothening nor stress relaxation is observed at low doses, and compressive stress, rather than tensile stress, is generated at high dose. The schematic drawing in Fig. 9 helps us to understand this behavior. As in the other cases, the implanted ions do not penetrate the whole film, so that the process of local melting and resolidification occurs only above a certain depth. The lattice at the depth of penetration, therefore, provides the template on which the resolidifying Zr nucleates, and thus it can cause strain in close analogy to liquid-phase epitaxial growth. Since this region is in a state of compressive stress according to Fig. 9 [$\sigma \lesssim 0.4$ GPa (Ref. 20)], the irradiated region also becomes under compressive stress. We thus identify the exponential convergence of the stress at high doses in Fig. 8 as a progressive modification of the lattice constant of the irradiated region towards its value at the depth of ion penetration. It is uncertain, however, whether the final stress at $\approx 5 \times 10^{15}$ represents a saturation value, or whether it eventually becomes tensile at still higher doses, as observed for the amorphous, nanocrystalline, and, as it will be seen, single-crystalline samples.

The above discussion also clarifies why grain growth and surface smoothening are inhibited in this structure during

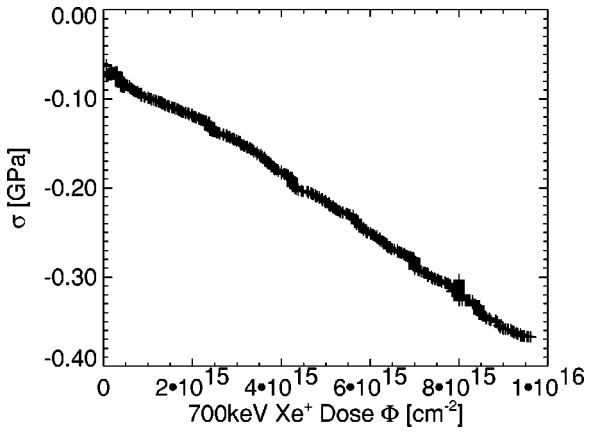

FIG. 10. Evolution of the average biaxial film stress of Nb single-crystal films during bombardment with 700 keV Xe^+ ions: The initial tensile stress of the film does not relax, but increases with irradiation dose.

irradiation. Grain growth is prevented because melted grains are nucleating on the preexisiting columnar grains, and the surface roughness is controlled by the force equilibrium between the surface and grain boundary energies [Fig. 9(a)].

The reason for the increase in the tensile stress at low doses is presently uncertain, but we tentatively attribute this behavior to the densification of the columnar grain boundary structure during irradiation. It is known that this structure is not fully dense and a similar densification behavior is observed during thermal annealing.[46]

VII. STRESS MODIFICATION OF SINGLE-CRYSTAL FILMS

A. Experimental results

Ion-beam-induced stress modification was also examined in a single-crystalline metal, Nb, using 700 keV Xe^+. The results for the evolution of stress are shown as a function of irradiation dose in Fig. 10. Initially the film is under slight tensile stress, arising from the differential thermal expansion of Nb and sapphire during cooling from the temperature at which dislocations become immobile to the ambient temperature. Similar to our other irradiations, the ion beam does not penetrate through the film. The irradiation does not lead to stress relaxation in this case, but rather to a nearly linear intensification of stress with dose from a small initial tensile stress of -0.05 GPa to a stress of ≈ -0.38 GPa at a dose of 1.0×10^{16} cm^{-2}. No indications of saturation are observed. This behavior can be partially understood by estimating the saturation stress using Eq. (4): We obtain a value of ≈ -3.2 GPa. Since this value is much larger than the value measured at the highest dose, it appears that the sample remains far from saturation even at our highest dose. AFM measurements of the surface morphology do not show significant deviations from an atomically smooth film, either before or after ion bombardment.

B. Simulations and discussions

As a model system for simulating irradiation-induced stress modifications in single-crystalline metals, we selected Cu, since past work had indicated that EAM potentials are reliable for this purpose.[17] The results are shown in Fig. 4. Bombardment leads to an increase in the initially compressive stress for 100 eV recoils, but no detectable change for the 5 keV events. The behavior at low energies is due simply to point defect generation. An analysis of defect production on two independent series of 50 (100 eV) events shows an average point defect concentration of 0.069% vacancies and 0.059% interstitials. The concentrations after 50 (5.0 keV) events are 0.35% vacancies, with 44% of these in the form of vacancy loops, and 0.089% interstitials, with no loops. While these concentrations are close to that expected for the 100 eV events, using a displacement energy of 29 eV,[1] they are significantly lower than what would be expected for the 50 (5 keV) events.[47] The latter fact, together with the imbalance of interstitials and vacancies, is a strong indication that both recombination and loss of defects to the open surface had occurred. Using the relaxation volumes of point defects deduced for our potential, we estimate the expected stress changes to be 0.046 GPa and 0.006 GPa for 100 eV and 5 keV recoils, respectively.

This agrees very well with the simulation results in Fig. 4 (0.008 GPa and 0.043 GPa for 100 eV and 5 keV recoils, respectively), but is in contrast to the experimental data on Nb, where strong tensile stresses are generated. In comparing the simulations of Cu with the experiments, we first note that stress relaxation is, indeed, not observed for either the 100 eV or 5 keV recoil events, i.e., RIV does not occur in the crystalline matrix. All changes in stress at low dose can be attributed to the addition of point defects. At high doses, the experiments show an increase in tensile stress that is not observed in the 5 keV simulations. On the other hand, the simulations reveal that there is an imbalance between vacancies and interstitials, with four times as many vacancies as interstitials. The difference can only be explained by the flow of mass to the surface. In fcc metals, however, the relaxation volume of the interstitial is nearly 10 times larger than that for a vacancy (2 times larger if the vacancy is in a loop). Consequently, the stress has not changed in this case even though mass does flow to the surface. For the 100 eV recoils, for which thermal spikes do not occur and there is little loss of atoms to the surface, the stress, in fact, increases. The experiments, however, clearly illustrate that tensile stresses are created. There are two important differences between the experiments and the simulations, the doses and the recoil energy. For the Xe irradiations of Nb, significant stresses develop only after a dose of 1.0×10^{15} cm^{-2}, or $\approx$10 dpa (assuming a displacement energy of 25 eV), while the simulation events produce a total of $\approx$0.02 dpa. Thus, we can expect the imbalance between vacancies and interstitials to increase with continued bombardment. The second difference is the recoil energy. For 700 keV Xe ions, the thermal spikes extend some tens of nm and this enables flow to the surface over longer distances. Although the importance of this effect is more difficult to quantify, it is clear that the larger melt volumes will increase the flow of atoms to the surface relative to creation of Frenkel pairs.[48]

It is interesting that the simulations on CuTi and AgNi did show the creation of tensile stresses at similar doses as em-

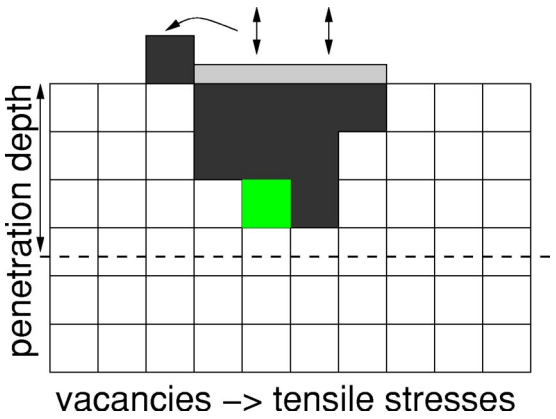

FIG. 11. Point defect creation within a collision cascade determines the stress modification of single-crystal films during ion bombardment.

ployed for Cu. For amorphous CuTi, however, it has been shown that the creation of a ''Frenkel pair'' by a recoil event has zero net volume change, since adding an atom has a relaxation volume of one atomic volume and removing an atom has a relaxation volume of negative one atomic volume. The loss of atoms to the surface, therefore, is not compensated by a larger relaxation volume of an interstitial atom. For NiAg, the grain size is less than 2 nm, and therefore, it is likely that any created interstitials would be immediately lost to a grain boundary, where its relaxation volume is certainly reduced. Thus, in this case also, the loss of atoms to the surface would not be compensated by the large relaxation volume of a small number of interstitials.

The picture that emerges for stress modification by cascades in single-crystal films is summarized in Fig. 11. At very low doses and low temperatures, compressive stress develops owing to the creation of Frenkel pairs. At higher doses, flow of mass to the surface results in an excess of vacancies below the surface, extending to the depth of the ion penetration, and these vacancies tend to form of dislocation loops. Interstitial atoms, moreover, are annihilated by the large excess of vacancies. The final stress results from the vacancy loops and therefore it is tensile.

VIII. CONCLUSIONS

In the present work we investigated the effects of the microstructure of thin films on the evolution of the mechanical stresses and surface morphology during ion bombardment. It appears that independent of the microstructure the effective film kinetics decelerates at high enough doses, reaching a steady state in the thin film kinetics during ion irradiation. We have clearly not reached this state for the single-crystalline sample, Nb, and possibly not for polycrystalline Zr as well, presumably because the final doses were smaller in these cases. The steady state is largely determined by the flow of mass onto the surface, creating tensile stresses, although in the case of crystalline samples, such as polycrystalline columnar Zr, the growth history of the film can define a reference state, which is eventually reached due to crystal lattice constraints. The contribution of mass flow to the final stress state can be estimated by a simple model based on thermal expansion during resolidification of the melt.

The development of the stress state in an irradiated metal at lower doses is more complicated and depends sensitively on the microstructure of the system. For amorphous alloys, the behavior is rather simple, as the system undergoes Newtonian viscous flow so that any gradients in the stress state are quickly relaxed. Nanocrystalline materials appear to undergo similar behavior, although the greater complexity of the microstructure introduces other considerations in the kinetic response, such as grain growth and grain rotation. In both cases, however, relaxation of the condition of conserving lattice sites enables viscous flow.

The response of the single-crystalline sample is also rather simple. The constraint of the crystalline lattice prevents changes in stress in the bulk material, other than a small contribution arising from the production of point defects. Thus, the stress state in single-crystalline materials is determined principally by the flow of mass onto the surface and the creation of tensile stress. Polycrystalline materials presumably behave similar to single crystals, except in the case when the structure initially has a depth-dependent stress state, as is the case for columnar Zr. Here, the process of melting and refreezing appears to act like liquid phase epitaxy with the film acquiring the stress state of the sample at the penetration depth of the implanted ions.

While the transient and final stress states in irradiated metals depends on the initial microstructure of material, we can conclude, however, that in all cases stresses changes derive from the kinetics of the melting and refreezing behavior on the nanomater scale of a thermal spike.

ACKNOWLEDGMENTS

We acknowledge Prof. Dr. C. P. Flynn, Department of Physics, University of Illinois at Urbana-Champaign, for providing us with Nb single crystal films. This material is based upon work supported by the U.S. Department of Energy, Division of Materials Sciences under Grant No. DEFG02-91ER45439, through the Frederick Seitz Materials Research Laboratory at the University of Illinois at Urbana-Champaign, as well as the Deutsche Forschungsgemeinschaft, SFB 602, Göttingen, TP B3. Part of the experimental research was carried out in the Center for Microanalysis of Materials, University of Illinois at Urbana-Champaign, which is partially supported by the U.S. Department of Energy, also under Grant No. DEFG02-91-ER45439. We are grateful for grants of computer time from the National Center for Supercomputing Applications (NCSA), the National Energy Research Scientific Computing Center (NERSC) and the Gesellschaft für wissenschaftliche Datenverarbeitung Göttingen, Germany (GWDG).

*Electronic address: smayr@uni-goettingen.de
†Electronic address: averback@uiuc.edu

[1] R.S. Averback and T.D. de la Rubia, Solid State Phys. **51**, 281 (1998).
[2] G. Martin and P. Bellon, Solid State Phys. **50**, 189 (1997).
[3] S.G. Mayr and R.S. Averback, Phys. Rev. Lett. **87**, 6106 (2001).
[4] P. Bellon, S.J. Chey, J.E.V. Nostrand, M. Ghaly, and R.S. Averback, Surf. Sci. **339**, 135 (1995).
[5] M. Morgenstern, T. Michely, and G. Cosma, Philos. Mag. A **79**, 775 (1999).
[6] C.C. Umbach, R.L. Headrick, and K.-C. Chang, Phys. Rev. Lett. **87**, 246104 (2001).
[7] C.A. Volkert, J. Appl. Phys. **70**, 3521 (1991).
[8] E. Snoeks, A. Polman, and C.A. Volkert, Appl. Phys. Lett. **65**, 2487 (1994).
[9] S.G. Mayr, Y. Ashkenazy, K. Albe, and R.S. Averback, Phys. Rev. Lett. **90**, 055505 (2003).
[10] M.L. Brongersma, E. Snoeks, and A. Polman, Appl. Phys. Lett. **71**, 1628 (1997).
[11] M. Jaouen, J. Pacaud, and C. Jaouen, Phys. Rev. B **64**, 144106 (2001).
[12] P. Ehrhart and W. Schilling, Phys. Rev. B **8**, 2604 (1973).
[13] G.W. Arnold, Nucl. Instrum. Methods Phys. Res. B **65**, 213 (1992).
[14] S. Klaumunzer and G. Schumacher, Phys. Rev. Lett. **51**, 1987 (1983).
[15] P. Jung, J. Appl. Phys. **86**, 4876 (1999).
[16] H. Trinkaus, J. Nucl. Mater. **223**, 196 (1995).
[17] T.D. de la Rubia, R.S. Averback, R. Benedek, and W.E. King, Phys. Rev. Lett. **59**, 1930 (1987).
[18] While it has been recently shown that viscous relaxation does not require melting, but can proceed simply from the creation of defects (Ref. 9), the same basic concept of radiation-induced viscous flow remains valid.
[19] S.G. Mayr and K. Samwer, Phys. Rev. Lett. **87**, 036105 (2001).
[20] S.G. Mayr and K. Samwer, Phys. Rev. B **65**, 115408 (2002).
[21] R.W. Hoffman, in *Physics of Thin Films: Advances in Research and Development* (Academic Press, New York, 1966), p. 211.
[22] F. Spaepen, Acta Mater. **48**, 31 (2000).
[23] S.M. Durbin, J.A. Cunnigham, M.E. Mochel, and C.P. Flynn, J. Phys. F: Met. Phys. **11**, L223 (1981).
[24] C.P. Flynn, W. Swiech, R.S. Appleton, and M. Ondrejcek, Phys. Rev. B **62**, 2096 (2000).
[25] S.G. Mayr and K. Samwer, J. Appl. Phys. **91**, 2779 (2002).
[26] A.I. van Sambeek and R.S. Averback, in *Ion-Solid Interactions for Materials Modification and Processing. Symposium.*, edited by D.B. Poker, D. Illa, Y.-T. Cheng, L.R. Harriott, and T.W. Sigmon (Mater. Res. Soc., Pittsburgh, PA, USA, 1996).
[27] G. Stoney, Proc. R. Soc. London **A82**, 172 (1909).
[28] W. Brantley, J. Appl. Phys. **44**, 534 (1973).
[29] SRIM 2000 computer code; see Ref. 35 for details.
[30] Also the implantation of inert gases into the metal films leads to generation of compressive stresses. Even for the highest irradiation doses, however, they are an order of magnitude smaller than measured stresses.
[31] This energy is typically required to create unstable point defects and is lower than the energy for creation of stable point defects.
[32] MD code; see, e.g., Ref. 47.
[33] H.J.C. Berendsen, J.P.M. Postma, W.F. van Gunsteren, A. DiNola, and J.R. Haak, J. Chem. Phys. **81**, 3684 (1984).
[34] M.S. Daw, S.M. Foiles, and M.I. Baskes, Mater. Sci. Rep. **9**, 251 (1993).
[35] J.F. Ziegler, J.P. Biersack, and U. Littmark, *The Stopping and Range of Ions in Matter* (Pergamon, New York, 1985).
[36] M.J. Sabochick and N.Q. Lam, Scr. Metall. Mater. **24**, 565 (1990).
[37] S.M. Foiles, Phys. Rev. B **32**, 3409 (1985).
[38] S.G. Mayr and R.S. Averback, Phys. Rev. B **68**, 075419 (2003).
[39] S.G. Mayr, M. Moske, and K. Samwer, Phys. Rev. B **60**, 16 950 (1999).
[40] The noise in the stress data, which is observed for high doses, originates from fluctuations in the ion fux of the accelerator. For high doses the integration time constant of the capacitance measurement was increased, leading to a reduced noise level.
[41] B. Reinker, H. Geisler, M. Moske, and K. Samwer, Thin Solid Films **275**, 240 (1996).
[42] A. Witvrouw and F. Spaepen, J. Appl. Phys. **74**, 7154 (1993).
[43] O. Müller, Diplomarbeit, Augsburg (1996).
[44] J. Frenkel, J. Phys. (USSR) **9**, 385 (1945).
[45] M. Weiss, M. Moske, T. Lorenz, and K. Samwer, Defect Diffus. Forum **129-130**, 181 (1996).
[46] P. Chaudhari, J. Vac. Sci. Technol. **9**, 520 (1972).
[47] K. Nordlund and R.S. Averback, Phys. Rev. B **56**, 2421 (1997).
[48] K. Nordlund, J. Keinonen, M. Ghaly, and R.S. Averback, Nature (London) **398**, 49 (1999).